International Journal of Greenhouse Gas Control 10 (2012) 199–214

Contents lists available at SciVerse ScienceDirect

International Journal of Greenhouse Gas Control

journal homepage: www.elsevier.com/locate/ijggc

Developing a robust geochemical and reactive transport model to evaluate possible sources of arsenic at the CO_2 sequestration natural analog site in Chimayo, New Mexico

Hari Viswanathan[a,*], Zhenxue Dai[a], Christina Lopano[b], Elizabeth Keating[a], J. Alexandra Hakala[b], Kirk G. Scheckel[c], Liange Zheng[d], George D. Guthrie[b], Rajesh Pawar[a]

[a] Earth and Environmental Sciences Division, Los Alamos National Laboratory, United States
[b] Geological and Environmental Science Focus Area, National Energy and Technology Laboratory, United States
[c] National Risk Management Research Laboratory, U.S. Environmental Protection Agency, United States
[d] Earth Sciences Division, Lawrence Berkeley National Laboratory, United States

ARTICLE INFO

Article history:
Received 21 December 2011
Received in revised form 22 May 2012
Accepted 14 June 2012

Keywords:
Carbon sequestration
Shallow groundwater impacts
Geochemical modeling

ABSTRACT

Migration of carbon dioxide (CO_2) from deep storage formations into shallow drinking water aquifers is a possible system failure related to geologic CO_2 sequestration. A CO_2 leak may cause mineral precipitation/dissolution reactions, changes in aqueous speciation, and alteration of pH and redox conditions leading to potential increases of trace metal concentrations above EPA National Primary Drinking Water Standards. In this study, the Chimayo site (NM) was examined for site-specific impacts of shallow groundwater interacting with CO_2 from deep storage formations. Major ion and trace element chemistry for the site have been previously studied. This work focuses on arsenic (As), which is regulated by the EPA under the Safe Drinking Water Act and for which some wells in the Chimayo area have concentrations higher than the maximum contaminant level (MCL). Statistical analysis of the existing Chimayo groundwater data indicates that As is strongly correlated with trace metals U and Pb indicating that their source may be from the same deep subsurface water. Batch experiments and materials characterization, such as: X-ray diffraction (XRD), scanning electron microscopy (SEM), and synchrotron micro X-ray fluorescence (μ-XRF), were used to identify As association with Fe-rich phases, such as clays or oxides, in the Chimayo sediments as the major factor controlling As fate in the subsurface. Batch laboratory experiments with Chimayo sediments and groundwater show that pH decreases as CO_2 is introduced into the system and buffered by calcite. The introduction of CO_2 causes an immediate increase in As solution concentration, which then decreases over time. A geochemical model was developed to simulate these batch experiments and successfully predicted the pH drop once CO_2 was introduced into the experiment. In the model, sorption of As to illite, kaolinite and smectite through surface complexation proved to be the key reactions in simulating the drop in As concentration as a function of time in the batch experiments. Based on modeling, kaolinite precipitation is anticipated to occur during the experiment, which allows for additional sorption sites to form with time resulting in the slow decrease in As concentration. This mechanism can be viewed as trace metal "scavenging" due to sorption caused secondary mineral precipitation. Since deep geologic transport of these trace metals to the shallow subsurface by brine or CO_2 intrusion is critical to assessing environmental impacts, the effective retardation of trace metal transport is an important parameter to estimate and it is dependent on multiple coupled reactions. At the field scale, As mobility is retarded due to the influence of sorption reactions, which can affect environmental performance assessment studies of a sequestration site.

1. Introduction

Numerous comprehensive analyses have concluded that recent increases in average global temperature are likely a result of increased concentrations of CO_2 and other greenhouse gases in the atmosphere (IPCC, 2007). Storing CO_2 in geologic formations is one approach to mitigate excess anthropogenic CO_2 from centralized sources such as coal-fired power plants (Bachu, 2000). One concern about geologic sequestration is the possibility of CO_2 and brine leakage from the sequestration reservoir affecting overlying aquifers utilized for drinking water. For this reason, groundwater protection is of vital importance to carbon capture

* Corresponding author. Tel.: +1 5056656737; fax: +1 5056658737.
E-mail address: viswana@lanl.gov (H. Viswanathan).

1750-5836/$ – see front matter © 2012 Elsevier Ltd. All rights reserved.
http://dx.doi.org/10.1016/j.ijggc.2012.06.007

and storage (CCS) projects. Although CO_2 is not toxic in low concentrations, increased CO_2 concentrations in the shallow subsurface could decrease pH, potentially resulting in the mobilization of trace metals from aquifer minerals and subsequently increasing naturally occurring contaminants such as As, Pb and U (Xu et al., 2003, 2005; Kharaka et al., 2006; Zheng et al., 2009). Simply injecting large amounts of CO_2 into the subsurface could also displace large amounts of brine that could already contain elevated concentrations of toxic metals (Stauffer et al., 2011). While risk assessment of CCS requires quantitative information about the potential impact of CO_2 and brine leakage on overlying aquifers, the consequences of such leakage are largely unknown.

Characterizing the potential impacts of leakage of CO_2 from the primary sequestration reservoir to overlying aquifers is a difficult task since many of these systems are not well characterized. In addition, the relationship between the aqueous phase and solid phases are complex. Modeling efforts and parameter estimates are difficult to measure in the field or to reliably determine from small scale laboratory experiments. Keating et al. (2010) described three strategies that have been used to evaluate shallow groundwater impacts due to CO_2 leakage. The first approach is to directly monitor shallow groundwater chemistry at an existing engineered CO_2 storage or enhanced oil recovery site. However, these sites are chosen at locations where no leakage is expected. For example, pilot CO_2 storage projects typically have well defined caprocks and deal with small amounts of CO_2 compared to the eventual large amounts required for effective storage. Enhanced oil recovery sites maintain strict pressure control to prevent migration of CO_2 since there is a large economic incentive to not lose CO_2 at these sites. In addition, groundwater data from these sites are not as detailed as the information utilized in this study. A second approach would be to use geochemical modeling in tandem with samples of site mineralogy and aqueous geochemistry data to predict impacts caused by CO_2 leakage (Zheng et al., 2009; Apps et al., 2010). Zheng et al. (2009) is a largely theoretical study that focuses on Pb and As under reducing conditions. Their model included detailed surface complexation sorption reactions and kinetic mineral stability reactions. Zheng et al. (2009) concluded that sorption was more important than precipitation–dissolution reactions. Apps et al. (2010) conducted systematic evaluation of possible water quality changes in response to CO_2 intrusion into aquifers currently used as sources of potable water in the United States. Their modeling study concluded that significant increase in As and Pb could result after the intrusion of CO_2 from a storage reservoir to a shallow confined groundwater resource, but the values remained below the specified maximum contaminant levels (MCLs). Studies such as Zheng et al. (2009) and Apps et al. (2010) can help identify the physical and chemical processes that may affect the impact of CO_2 intrusion at a particular site. However, the predicted impacts will be qualitative in nature due to large uncertainties in mineralogy, aqueous geochemistry, chemical kinetics, and chemical–physical heterogeneity. No comparisons of simulation to water chemistry measurements were provided in these studies.

Continuing with the approaches proposed in Keating et al. (2010), we utilized the third approach which involves directly measuring CO_2 injection impacts at a natural analog site. As with the other two approaches, there are limitations. For example, pre-CO_2 and post-CO_2 conditions cannot be analyzed. However, natural analog sites can help study processes at the timescales of interest and allow comparison between field measurements, bench scale laboratory experiments and geochemical modeling. For this study the Chimayo site in northern New Mexico was selected, which is a location where CO_2 is actively upwelling though a shallow aquifer. Twenty groundwater wells are available for sampling this system. Keating et al. (2010) results show that a few of the wells have high concentrations of U, As and Pb. At certain locations, brine upwells without CO_2 provides an opportunity to isolate the impact of CO_2 on water quality. The data shows there is evidence that As, U and Pb are locally co-transported into the aquifer with CO_2-rich brackish water. As originated from deep groundwater but over time As has accumulated in various aquifer sediments in the shallow subsurface. In this study, experiments were designed to expand upon prior work to examine the mechanistic processes that control the migration of a trace metal, specifically As, at the Chimayo site. The upwelling data of Keating et al. (2010) explains some but not all trace metal observations. In this work, we focus on processes such as sorption and precipitation/dissolution that control trace metal migration in the shallow subsurface. Arsenic was chosen as the target element since it exceeds the MCL at several wells and Apps et al. (2010) noted it as a possible concern at potential CO_2 sequestration sites across the United States.

In order to identify the mechanisms controlling As transport at this site, several complementary techniques were applied. These include a statistical analysis of previously reported groundwater quality data, detailed geochemical and mineralogical analyses of outcrop samples from the site, experiments exposing aquifer samples to CO_2 in the laboratory, and reactive-transport modeling. First, water quality data from the twenty wells at the site were used to look for statistical trends to indicate similarities or differences between As concentrations and other analytes. Aquifer samples from the Chimayo site were analyzed using X-ray diffraction (XRD), scanning electron microscopy (SEM), and energy dispersive spectroscopy (EDS) to determine mineralogy, evaluate particle morphology, and identify potential arsenic-bearing phases. Synchrotron micro X-ray fluorescence (μ-XRF) was utilized to map the trace metal distribution within various fractions of the Chimayo sediment samples. Batch experiments were designed to investigate the role of sorption and mineral formation reactions, redox conditions, and factors that affect the transport of As in the shallow subsurface Chimayo groundwater. These experiments were conducted by exposing the samples to CO_2 to determine if trace elements are released. Using the information gathered from these methods, a geochemical model of the system was constructed. Finally, a one-dimensional flow path simulation was derived to represent field-scale migration at the site to determine the mechanistic processes controlling the fate of As in a reactive transport system. The goal of this study was to determine which reaction mechanisms control the fate of As at Chimayo.

2. Site and sample description

Keating et al. (2010) describes the hydrogeological and geochemical settings for the Chimayo site in detail; therefore, only a summary is provided in this manuscript. Chimayo, New Mexico, lies in north-central New Mexico in the semi-arid Espanola basin. Aquifer sediments at the site are comprised of quartz, plagioclase, calcite and clay minerals. Rock-water interactions, such as chemical weathering, explain trends in major ion chemistry with dissolved species generally increasing with depth (Hereford et al., 2007; Keating and Warren, 1999). Cumming (1997) sampled wells in the Chimayo community and observed that shallow wells (depth < 60 m) located near the Roberts Fault are enriched in dissolved CO_2. A geochemical data set was created from 18 wells, most of which were sampled four times over a two year period (Fig. 1a). Keating et al. (2010) expanded the number of domestic drinking water wells originally sampled by Cumming (1997). The analyses also included trace elements and stable isotopes (^{13}C, ^{18}O, ^{2}H). Since many wells have been abandoned since the sampling conducted by Cumming (1997), of the 18 wells sampled in this study only four were also sampled by Cumming (1997). The trace metal and major ion chemistry data collected by Keating et al. (2010)

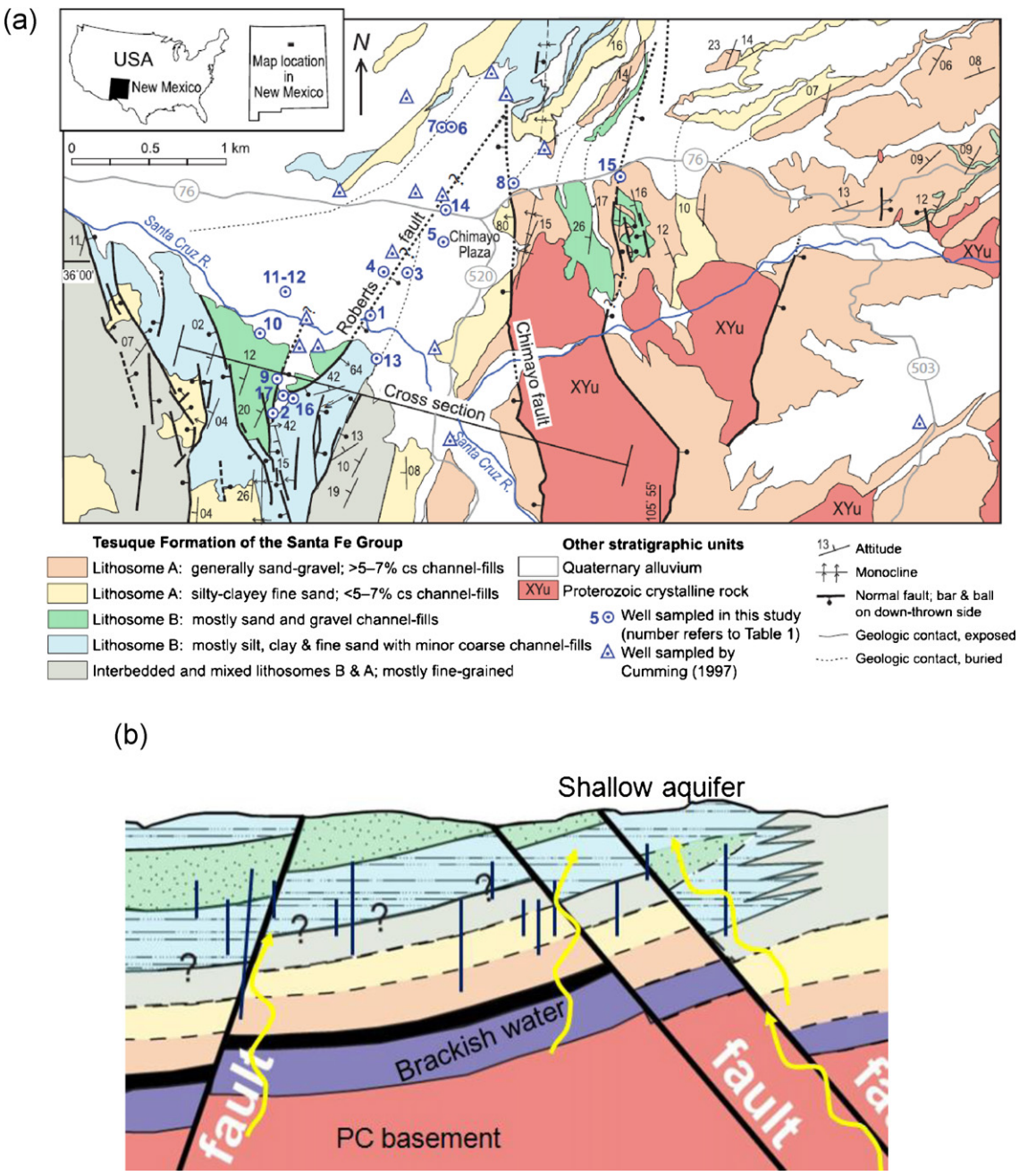

Fig. 1. (a) Map of Chimayo surface geology and well locations as shown in Keating and Warren (1999). (b) The conceptual model of CO_2 rises from deep aquifer along faults in the Chimayo site.

were used in this study in order to statistically evaluate trends in the trace metal data. Chimayo aquifer sediments used for trace element characterization and experimental work were collected during March 2009 from outcrops of the primary sedimentary layers identified in Keating et al. (2010), and groundwater samples for Fe measurements were collected during August 2009. Of these samples, sediments from the "Roadcut Lithosome B" aquifer outcrop were used for characterization and experimental work unless otherwise noted. This section of the aquifer contains the highest concentration of As relative to the other samples (Table 1a), and is composed of a mix of sandy and clayey materials (Table 1b). There was an attempt to mitigate the impacts of weathering of the sediments by removing surface material to access more pristine deeper material in the outcrop. Fig. 1b describes the conceptual model developed for the site in which CO_2 rises from the deep aquifer along fault zones. Observation wells close to the faults therefore have high values of dissolved CO_2 whereas wells far from the faults are not rich in dissolved CO_2. These trends allow determination of the impact of CO_2 on trace element concentrations at the site. In the next section, statistical techniques are described to interpret the data from the observation wells.

3. Statistical analysis of field data

A statistical analysis of the Chimayo observation well data was conducted to determine if there are correlations between the key

Table 1a
Total As concentrations by aqua regia digestion and ICP-MS analysis for Chimayo aquifer outcrop samples. Designation as "roadcut" or "streamcut" indicates the outcrop location sampled, and the lithosomes identified correspond with those shown in Fig. 1a.

Sample	[As] (mg/kg)
Roadcut Lithosome A (Combined)	14.0
Roadcut Lithosome A (Gray Isolate)	5.0
Roadcut Lithosome A (Red Isolate)	16.7
Roadcut Lithosome B	147.0
Streamcut Lower Lithosome B	82.0
Streamcut Lithosome B	69.1

aqueous geochemical parameters such as chloride, pH, Eh, and As. Strong correlations could provide additional lines of evidence for which reactions and transport processes are occurring. Trends in the observed concentration data can be quantified with statistical methods. In order to interpret the relationship between chemical species in different monitoring wells, the correlation coefficients amongst aqueous species were calculated. These results can help analyze the geochemical conditions and build the conceptual models for As reactions for this site. For example, the correlation between two species, which are located in the same aquifer, can provide information about the source and reaction mechanisms between the two species.

In this data set, there are concentration observations of 20 chemical species from 18 monitoring wells (Keating et al., 2010). The MCL for As is 0.01 mg/L (EPA, 2009). The mean concentration of 0.0031 mg/L for As at the Chimayo site is still lower than the MCL; but, at Well 17 and Well 15, the measured As concentrations are higher than the MCL. Field trends in the data provided no clear explanation for why As was high at these locations. There are no specific spatial or geochemical characteristics in the wells with elevated As readings. The correlation analysis indicates that the aqueous As concentration is strongly positively correlated with the concentrations of Pb and U, and these three trace elements may be from the same source or same transport pathway (Fig. 2). These elements are also correlated to chloride indicating that co-transportation with upwelling brine is a possibility. There is no strong correlation between As and alkalinity, which could indicate that high dissolved CO_2 does not affect the dissolution/precipitation of arsenic-bearing minerals due to the oxidizing condition at the Chimayo aquifer. This conclusion is similar to the analysis of Keating et al. (2010) in which co-transportation with brine and not high CO_2 concentrations was found to be a likely transport mechanism for As, U and Pb for high salinity waters.

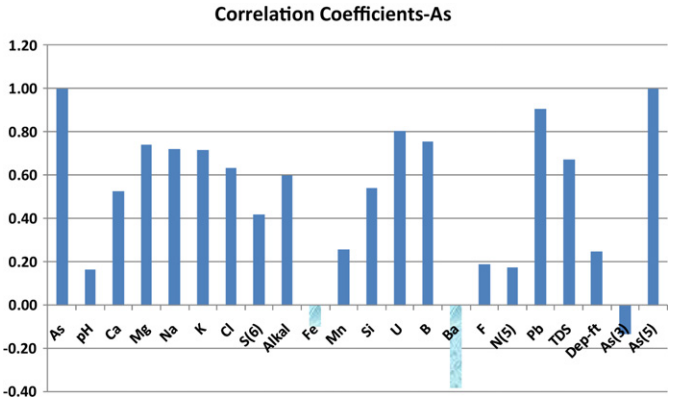

Fig. 2. Correlation coefficients of total aqueous arsenic related to other chemical species and depth.

4. Experimental techniques and characterization

Expanding on the aqueous geochemistry characterization efforts from Keating et al. (2010), experimental and characterization efforts were focused towards evaluating As speciation and distribution in Chimayo aquifer sediments, and CO_2-induced release of As from Chimayo sediments. Based on the need for more comprehensive data to ascertain the cause of the trends described in the previous section, experimental and geomaterials characterization techniques were employed to evaluate As distribution in these samples, and to evaluate its behavior in the presence of CO_2. Chemical extractions were performed to determine the total amount of As present in the samples, and experiments were conducted to react the Chimayo aquifer sediments in CO_2-charged synthetic groundwater solutions to evaluate changes in aqueous chemistry related to reactions with CO_2. These lines of geochemical data were coupled with SEM, XRD and μ-XRF mapping to discern sources of As in the Chimayo sediments. The ultimate goal for these comprehensive analyses was to use the resulting data to define a suite of geochemical processes controlling As behavior in the CO_2-affected Chimayo aquifer system that then can be used as inputs for geochemical and reactive transport modeling.

Table 1b
Quantitative XRD analysis results (weight %) for the mineralogy of the Chimayo aquifer outcrop samples.

Phase	General chemical composition	Sample					Average weight fraction
		Roadcut Lithosome B	Roadcute Lithosome A (Gray Isolate)	Roadcut Lithosome A (Red Isolate)	Streamcut Lithosome B	Streamcut Lower Lithosome B	
Quartz	SiO_2	26	48.1	42.3	54	38.8	0.437
K-feldspar	$KAlSi_3O_8$	3.6	6.7	5.6	5.5	4.6	0.055
Plagioclase[a]	(Na, Ca) (Al, $Si)_4O_8$	4.8	10.8	8.9	15.6	5.7	0.047
Calcite	$CaCO_3$	0.4	4.7	1.8	0.6	1.6	0.019
Hematite	Fe_2O_3	0.4	–	0.1	0.5	0.3	0.002
Illite/mica	$K_{0.60.85}$(Al, Mg, $Fe)_2$ (Si, $Al)_4O_{10}(OH)_2$	43.4	20.3	29.5	11	29.4	0.285
Kaolinite	$Al_2Si_2O_5(OH)_2$	1.5	–	0.1	0.3	0.9	0.008
Smectite	$(Na, Ca)_{0.3}$(Al, $Mg, Fe)_{2-3}$ (Si, $Al)_4O_{10}$ $(OH)_2{\cdot}nH_2O$	20.2	9.3	11.6	12.5	18.8	0.148

[a] For modeling purposes, the plagioclase concentration was assumed to be split equally between the albite ($NaAlSi_3O_8$) and anorthite ($CaAl_2Si_2O_8$) end-members.

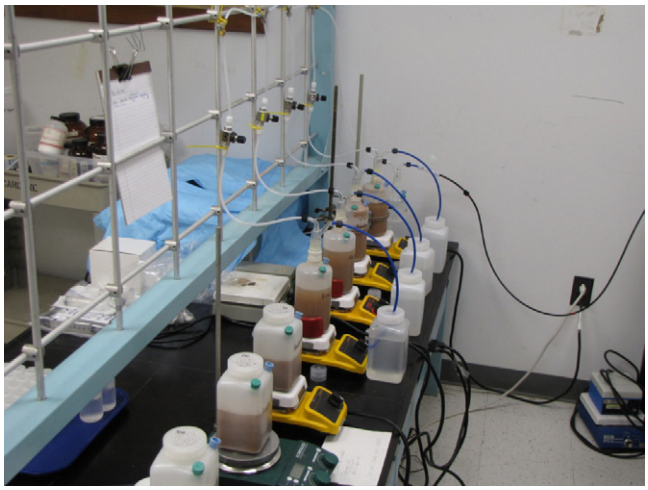

Fig. 3. Reactor bottles containing Chimayo roadcut sediment, synthetic groundwater, and lines for CO_2 introduction. Reactors without incoming gas lines were used for the steady-state, CO_2-free control experiments.

4.1. Digestions and batch experiments

Aqua regia digestions were performed on 6 samples collected from various sedimentary layers within the Chimayo aquifer. The aqua regia digestions were performed by reacting 0.5 g of dry sample with an aqua regia solution (1 mL trace metal grade nitric acid and 3 mL trace metal grade hydrochloric acid, diluted to volume with distilled, de-ionized water) in a Pyrex flask on a heated stir plate for 5 h. Arsenic concentrations in the resulting supernatant were analyzed via inductively coupled plasma mass spectrometry (ICP-MS). Results show that As concentrations range from 5 to 147 mg/kg (Table 1a).

Batch experiments were conducted to mimic the influx of CO_2 into the aquifer in order to evaluate CO_2-specific effects on As behavior due to reactions between Chimayo aquifer sediments and elevated system CO_2. The experiments were designed to evaluate CO_2-specific effects on solution chemistry by performing a "CO_2-affected" experiment in parallel with a CO_2-free "control." Experiments modeled as part of this study (e.g. Section 5.2) were based on reacting the mixed clay/sand Chimayo sediment ("Roadcut Lithosome B") with synthetic groundwater generated in the laboratory roughly based on the major ion composition of Well 15 (to represent "background" groundwater chemistry) reported by Keating et al. (2010). Parallel experiments also were performed using the Roadcut Lithosome B sample and synthetic "saline" waters with total dissolved solids content similar to Well 17 reported by Keating et al. (2010), for comparison to experiments performed using the "background" water (although only the "background" water experiments were modeled in this study). Trace element concentrations were not included as part of the chemical recipe for these synthetic solutions; any existing trace elements are due to impurities in the salts used to make the solutions. Although our synthetic saline water chemistry differed slightly from the target composition (Well 17 from Keating et al., 2010), these experiments remain valuable for evaluating geochemical changes that may occur under high-TDS fluid leakage scenarios. For the two sets of experiments (background and saline), one reactor was exposed to hydrated CO_2, and one reactor was kept as a steady-state, CO_2-free control (Fig. 3). Aqueous sample aliquots were collected at designated time points, and CO_2 flow was stopped to allow suspended solids to settle within the experimental bottles prior to extracting sample aliquots. All reactors were allowed to reach a steady state between the solids and synthetic groundwater (3 days). After 3 days, CO_2 was introduced to reactors undergoing reaction with CO_2, and the initial time point for the experiments with CO_2 was collected after CO_2 was bubbled through the system for 1 h. Filtered (0.45 μm) and acidified (with trace metal grade HNO_3) aliquots were submitted for ICP-MS and ICP-Optical Emission Spectroscopic (OES) analyses; non-acidified samples were used to measure pH and for ion chromatography analyses. Although ICP-OES is able to detect most elements, As was also measured by ICP-MS techniques in order to determine concentration values that were below the detection limits of the ICP-OES instrument.

Experimental results showed that reactions with CO_2 started with high solution As concentrations at the initial sampling point relative to the steady-state controls for both the "background" and "saline" groundwater conditions. As the experiment progressed with time, As concentrations decreased gradually to below instrument detection limits in both the CO_2-reacted "background" and "saline" groundwater solutions (Fig. 4).

4.2. X-ray diffraction

XRD was performed in order to evaluate the mineralogy of the Chimayo sediments. Each sample was ground and mixed with a corundum internal standard with a 80:20 weight ratio of sample:standard. XRD measurements were conducted on a Siemens D500 theta-theta diffractometer equipped with Cu Kα radiation. Data were collected from 2° to 70° 2θ in step scan mode with a step size of 0.02°, and count times of 8–12 s/step. Quantitative analyses were performed using the FullPat program described in Chipera and Bish (2002). Based on the XRD analyses of five samples collected from different locales in the Chimayo site, the mineral assemblages include quartz, K-feldspar, plagioclase, calcite, hematite, illite/mica, kaolinite, and smectite in varying amounts (Table 1b). There was no evidence for the presence of iron sulfides (e.g. pyrite, arsenopyrite, etc.) in any of the samples via XRD analyses.

4.3. Scanning electron microscopy

A small amount of unconsolidated "Roadcut Lithosome B" sediment was mounted onto SEM stubs using double-sided carbon tape, then carbon coated for analysis. A portion of the <100 mesh (<149 μm) sediment was also mounted in epoxy and prepared for thin section by Spectrum Petrographics. The thin sections were 30 microns thick and mounted on quartz glass slides. The thin section samples were used for synchrotron analysis as well as SEM analysis. The polished thin section provided a cross-section of the unconsolidated material. The grain mount samples and thin sectioned sediment samples were analyzed via SEM using a FEI-Quanta 600 FEG Environmental SEM (ESEM) equipped with an Oxford INCA energy dispersive spectroscopy (EDS) detector. The coated grain mounts were analyzed in High Vac mode at 20–30 kV and the thin section mounts were run uncoated in Low Vac mode at 15–20 kV. All samples were analyzed at a working distance of 10 mm.

SEM-EDS was used to evaluate the general morphology and chemistry of the Chimayo sediments. For this work, the analysis focused on the "Roadcut Lithosome B" sample, which contained the highest amount of bulk As (Table 1a). The sample was comprised primarily of quartz, feldspar, and clay materials (as confirmed by XRD analysis, Table 1b). The clay materials appear to coat various mineral grains, and also appear to be Fe-rich (Fig. 5a). In addition to being present as fine-grained coatings, the clays are also found as lathes within the sample (Fig. 5b). The clay lathes appear to be Mg- and Fe-rich (Fig. 5b). There was no evidence for Fe–S-rich particles in any of the samples analyzed via SEM-EDS. Arsenic was not detected via EDS in any of the samples due its trace concentration and the detection limitations of the instrument.

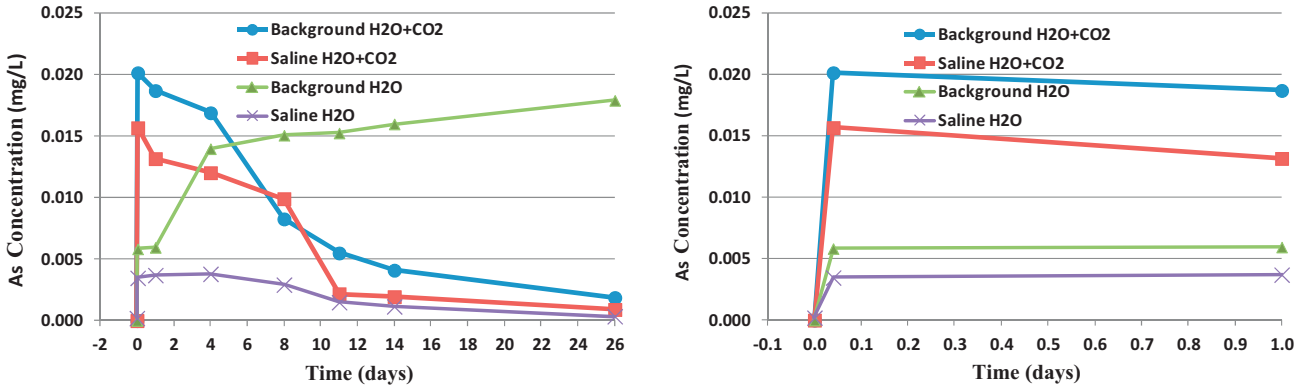

Fig. 4. As concentrations decreased gradually from the solutions in both the CO_2-reacted "background" and "saline" groundwater solutions during the batch experiments of Roadcut Lithosome B sample. Time $t = 0$ day represents the time at which CO_2 was added to the "Background $H_2O + CO_2$" and "Saline $H_2O + CO_2$" experiments. The first three measurements of As concentrations are plotted in the figure on the right hand side to show the concentration variations at early time of the batch experiments.

4.4. Synchrotron X-ray fluorescence mapping

EDS is effective for detecting major elements present in samples; however, in order to focus on the distribution of trace elements such as As, synchrotron X-ray microprobe measurements were conducted. Synchrotron micro X-ray fluorescence (μ-XRF) mapping was performed on thin sections of Chimayo sediments at GSECARS, beamline 13-1D, at the Advanced Photon Source (APS) of Argonne National Laboratory, Argonne, IL. The electron storage ring operated at 7 GeV with a top-up fill mode. Microprobe data were collected using a 4-element Silicon drift detector, a Si(1 1 1) monochromator, and 101 mA beam current. The elemental mapping was done with an incident beam energy of 17 or 19 keV with map areas up to 500 μm × 500 μm in size using a focused beam of approximately 2 μm × 2 μm. Two-dimensional image maps were collected for a variety of elements, including: K, Ca, Ti, Cr, Mn, Fe, Cu, Zn, As, Se, Rb, Sr, Y, Zr, Pb, and U, where possible. Data were analyzed to interpret the chemical distribution of potential contaminants (e.g. U, As, and Pb) with other elements. Sample maps can be found in Figs. 6 and 7.

In general trace metals such as Pb and As were correlated with Fe in most of the shallow Chimayo sediments (Fig. 6). U also trends with the Fe, but also showed correlation with Sr and K. Focusing on As for this paper, As illustrated a strong correlation with Fe in

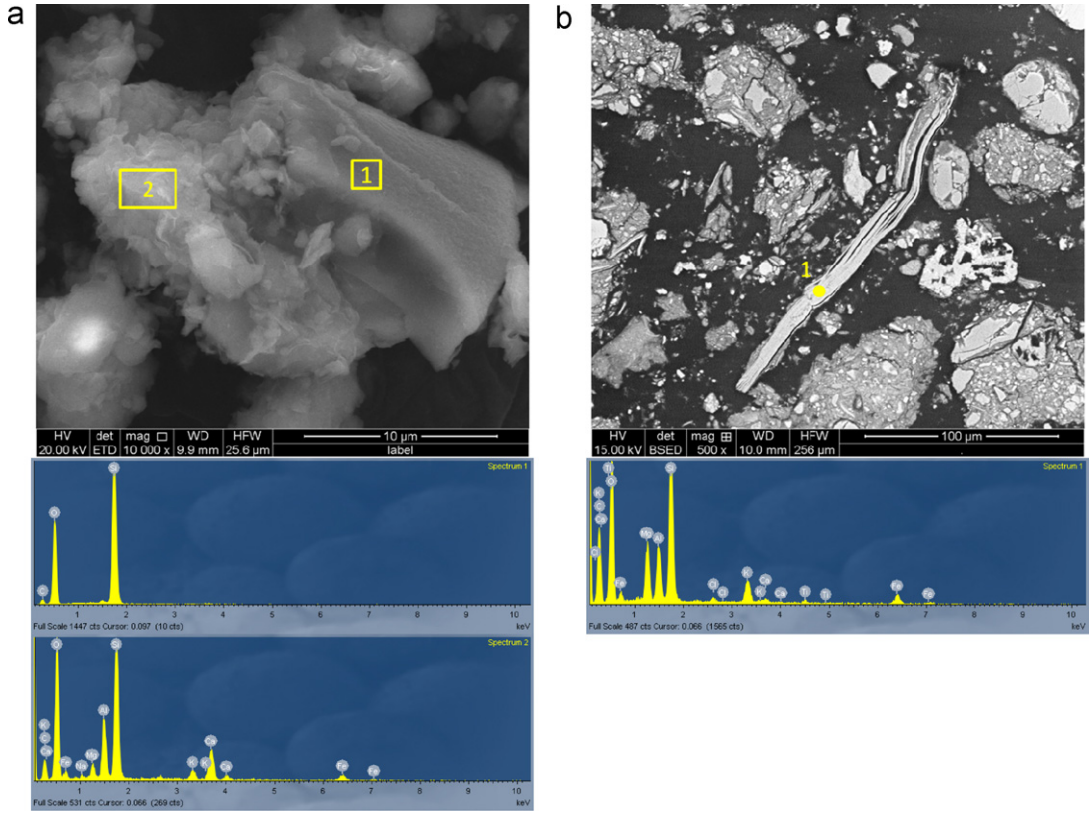

Fig. 5. Sample SEM-EDS images for sample "Roadcut Lithosome B", where (a) secondary electron image with corresponding EDS spectra (below) of particles in grain mount, and (b) back-scatter image with a corresponding EDS spectrum (below) of clay lathe in thin section. Based on both the morphology and chemical information shown in the spectra, this figure illustrates (a) a quartz (Si–O-rich) grain coated by fine-grained, agglomerated clay type material (Ca-, K-, Fe-, Mg-, Al-, Si-, O-rich), and (b) an isolated clay lathe (K-, Fe-, Mg-, Si-, Al-, O-rich).

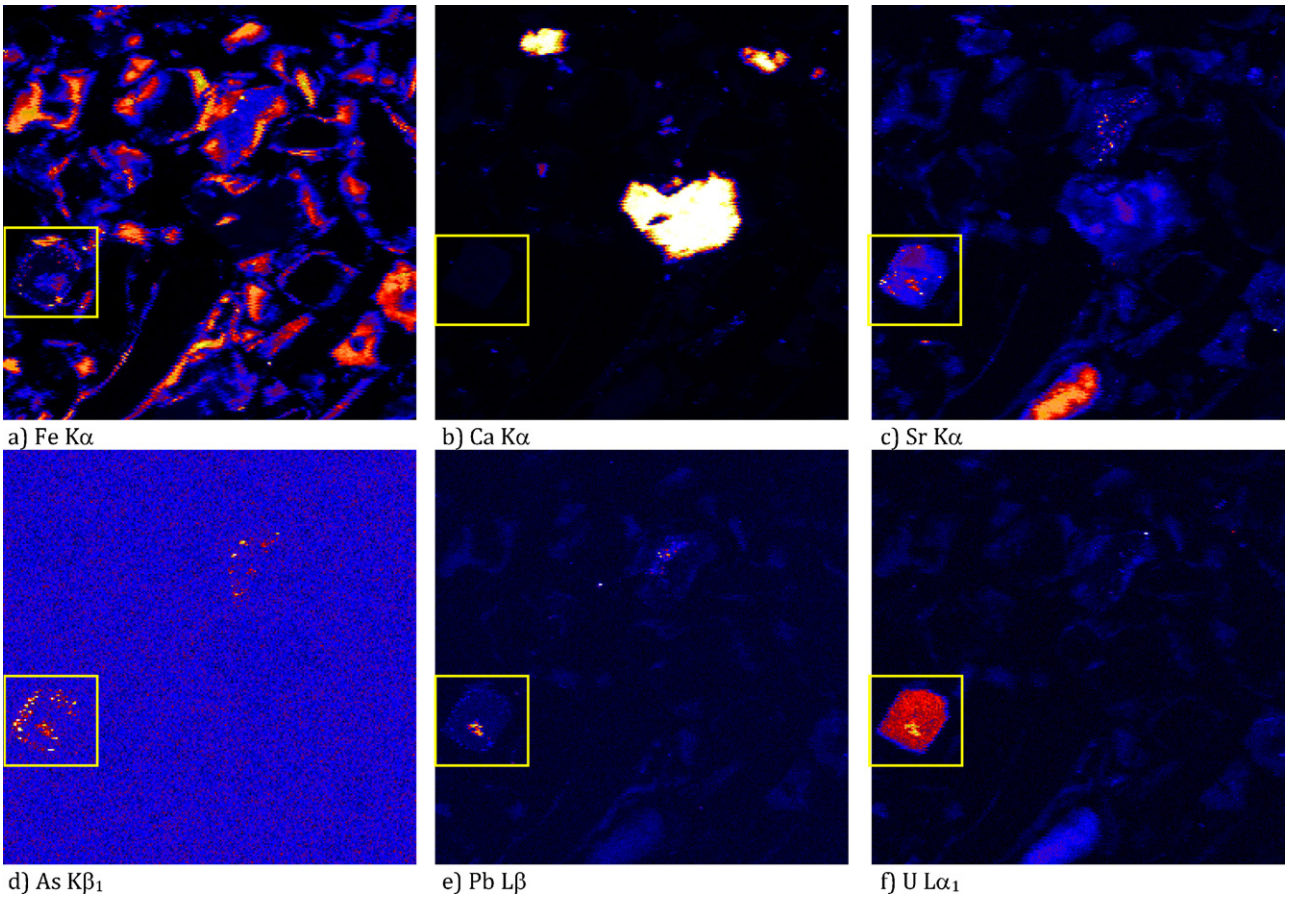

Fig. 6. Selected element distribution maps for sample Roadcut Lithosome A (Gray Isolate) illustrating that As, Pb, and U all show a general trend with Fe in this portion of the Chimayo sediment (particularly As and Pb). Uranium also shows a trend with Sr. A yellow box has been drawn around a particular area of interest in this map (warmer colors in the false color maps correspond to higher concentrations of each element). Maps were collected at 19 keV with a step size of 2 μm. Each map area is 500 μm × 500 μm. Sample was covered in kapton tape for analysis due to presence of U in the sample.

all Chimayo sediment thin sections analyzed (3 in total, "Roadcut Lithosome B", and both the gray and red fractions of "Roadcut Lithosome A"); however, it should be noted that while the trend with Fe is prominent, it is not absolute. Fig. 7 illustrates the Fe and As association in "Roadcut Lithosome B", which is the sample used for the experimental work reported above, and is the sample that contained the highest bulk concentration of As. Based on the XRD and SEM-EDS results for this sample, iron is present both in Fe-rich clays (illite and/or smectite) and as hematite (and/or iron oxyhydroxides). Thus, this implies that the As is associated with either the clay or oxide phases in the Chimayo sediments, most likely as an adsorbed species. Additional spectroscopy (X-ray Absorption

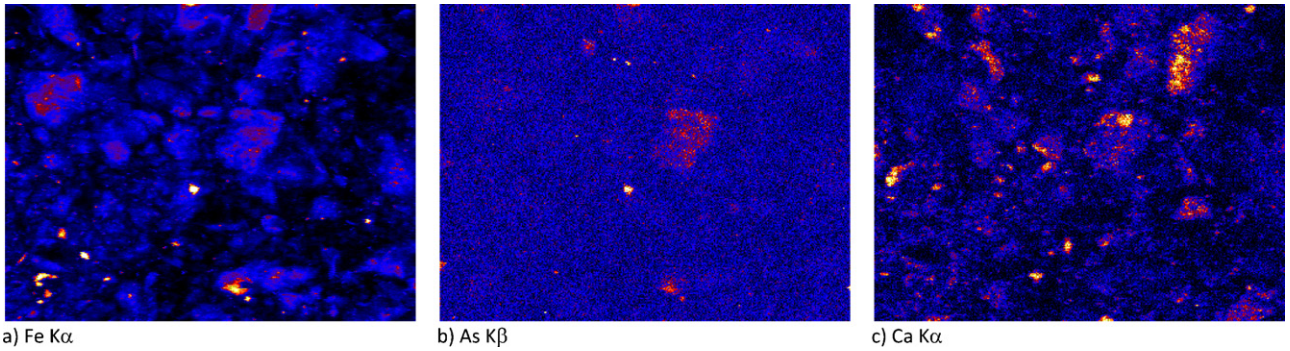

Fig. 7. Selected element distribution maps for (a) iron, (b) arsenic and (c) calcium, in a portion of sample Roadcut Lithosome B from the Chimayo site (warmer colors in the false color maps indicate higher concentrations of each element). Comparisons illustrate how arsenic tends to trend with iron for the most part; however, there are small regions where this is not the case. Maps were collected at 17 eV with a step size of 2 μm. Each map area in this figure is 350 μm × 270 μm. Al foil was used as a filter on the detector to prevent oversaturation; thus the light element (e.g. Ca) counts were reduced.

Table 2
Calculated pe values from Fe(II) data. [Fe(II)] values are derived from colorimetric measurements via the 1,10-phenanthroline method, [Fe]T values are from ICP-OES. The pe was calculated using Geochemists Workbench V7.0 with thermo.dat database. The upper end of the pe range is 12, based on dissolved O_2 measurements reported in Keating et al. (2010).

[Fe(II)] (μM)	[Fe]T (μM)	Calculated pe
3	8	4.3
2	10	7.1
35	132	7
209	626	5.5
9	224	5.5
0	5.3	12
0	7.7	12

Near-Edge Structure, XANES) is currently underway in order to directly evaluate the As and Fe speciation and binding environment in the Chimayo sediments.

4.5. Using field-measured Fe values to constrain system redox potential

Based on partial pressures of O_2 reported in Keating et al. (2010), the Chimayo aquifer is anticipated to be under generally oxidizing conditions with a pe around 12. In order to confirm the potential range of pe values in the aquifer, measured Fe(II) and total Fe was determined in groundwater collected from Chimayo wells. The 0.45-μm filtered groundwater samples were acidified with HCl for preservation, and Fe(II) concentrations were determined colorimetrically using the 1,10-phenanthroline technique, which has been used previously to measure natural water Fe(II) concentrations in the range of 10–1500 μM (Hakala et al., 2009). The total Fe and Fe(II) concentrations were used to calculate Fe(III) (estimated as the difference between total Fe and Fe(II)), and in the Chimayo groundwater samples ranged from 0 to 214 μM Fe(II). Redox potentials were calculated based on the Fe(II)/Fe(III) redox couple using Geochemists Workbench v.7.0. All calculations resulted in pe values ranging from 4 to 12. The calculated pe values shown in Table 2 contain some uncertainty in regards to whether they represent local Fe(II)/Fe(III) disequilibrium in the sampled wells, or if the system is actually at equilibrium with the Fe(II)/Fe(III) redox couple. Additionally, uncertainties may exist in the O_2 ranges reported previously. Regardless of these uncertainties, within the circumneutral pH of the Chimayo aquifer and across the calculated pe range of 4 to 12, As is expected to be present in the As(V) form.

5. Batch geochemical modeling

5.1. Constructing a geochemical model based on laboratory experiments

By using Phreeqc (Parkhurst and Appelo, 1999), an aqueous speciation analysis was conducted of all the groundwater observation data. A total of 44 aqueous complexes were selected that have concentrations high enough to impact the results. Table 3 lists the complexes and their equilibrium constants. Groundwater chemistry data from Well 15 was utilized since it is one of the wells in which the As concentration is higher than the MCL. The pe values were calculated based on groundwater collected at several wells after the Keating et al. (2010) analysis was conducted, as described in Section 4.5. All the wells had pe values greater than 4 and ranged between 4 and 12. Under these conditions As(V) is the dominant form in the aqueous phase with very little As(III) in solution. The modeled Phreeqc speciation results show that As in the shallow aquifer at Chimayo is mainly As(V) in the form of $H_2AsO_4^-$ and $HAsO_4^{2-}$ at a pH of 6.4 and pe of 4.

The speciation analysis also shows possible minerals at the site and their saturation indexes. Fig. 8 shows that all the As containing minerals are undersaturated and very far from equilibrium. Therefore mineral reactions with As bearing minerals are either very slow or nonexistent in the shallow subsurface. The XRD and SEM-EDS analyses did not detect any As bearing minerals, but it is possible they do they exist in very small amounts. It is possible that the deep water source of As in these waters is from dissolution of As bearing minerals near the basement rocks where reducing conditions are expected and minerals such as pyrite (and/or arsenopyrite) may be prevalent. While we do not believe As bearing minerals play an important role in the shallow subsurface, mineral precipitation/dissolution of non-arsenic bearing minerals are important in controlling the pH of the system. Precipitation/dissolution reactions for all minerals detected in the sample (Table 1b) were included in the geochemical model and precipitation of secondary minerals was allowed in order to constrain major ion chemisty in the system. Dissolution of quartz, K-feldspar and plagioclase consume H^+ and may impact pH, redox and As sorption onto the clay minerals. They are included in the geochemical model, along with hematite, calcite and clay mineral reactions. Since plagioclase mainly consists of albite and anorthite and the Toughreact database (Xu et al., 2006, 2011) only includes the later two minerals, we substituted plagioclase with these two minerals and assigned a half of the volume fraction of plagioclase to both albite and anorthite.

The kinetically controlled mineral dissolution/precipitation reactions that are likely to be important in the shallow aquifer sediments were selected based on the XRD analysis of the site. The Toughreact Version 2.0 database (Xu et al., 2006, 2011) was used to obtain equilibrium constants at 25 °C for these mineral reactions:

$$\text{Illite}: \quad 1.2H^+ + 0.25Mg^{2+} + 0.6K^+ + 3.5SiO_2(aq) + 0.4H_2O + 2.3AlO_2^- \quad \log(K) = -47.33$$

$$\text{Kaolinite}: \quad 2H^+ + 2SiO_2(aq) + H_2O + 2AlO_2^- \quad \log(K) = -39.82$$

$$\text{Smectite–Ca}: \quad 0.96H^+ + 0.26Mg^{2+} + 0.145Ca^{2+} + 3.97SiO_2(aq) + 0.52H_2O + 1.77AlO_2^- \quad \log(K) = -39.51$$

$$\text{Smectite–Na}: \quad 0.96H^+ + 0.26Mg^{2+} + 0.29Na^+ + 3.97SiO_2(aq) + 0.52H_2O + 1.77AlO_2^- \quad \log(K) = -39.53$$

$$\text{Calcite} + H^+: \quad Ca^{2+} + HCO_3^- \quad \log(K) = 1.85$$

$$\text{Hematite} + 4H^+: \quad 0.5O_2(aq) + 2H_2O + 2Fe^{3+} \quad \log(K) = -16.87$$

$$\text{Quartz}: \quad SiO_2(aq) \quad \log(K) = -3.74$$

$$\text{K-feldspar}: \quad K^+ + 3SiO_2(aq) + AlO_2^- \quad \log(K) = -22.91$$

$$\text{Albite}: \quad Na^+ + 3SiO_2(aq) + AlO_2^- \quad \log(K) = -20.12$$

$$\text{Anorthite}: \quad Ca^{2+} + 2SiO_2(aq) + 2AlO_2^- \quad \log(K) = -19.19$$

The rate constants of the above mineral reactions are fairly well known and published values exist in the Toughreact Version 2.0 database (Xu et al., 2006, 2011). These values were applied for

Table 3
Aqueous complexes and their equilibrium constants at 25 °C.

Species	Log K (25 °C)	Species	Log K (25 °C)	Species	Log K (25 °C)	Species	Log K (25 °C)
OH^-	13.99	$CaHCO_3^+$	−1.04	$CaOH^+$	12.85	$PbCl_3^-$	−1.70
Al^{3+}	−22.88	$MgHCO_3^+$	−1.03	NaOH(aq)	14.15	$PbCl_4^{2-}$	−1.50
$CaCl^+$	0.70	CO_2(aq)	−6.34	$NaCO_3^-$	9.82	$PbOH^+$	7.57
$CaCl_2$(aq)	0.65	CO_3^{2-}	10.33	$H_3SiO_4^-$	9.81	Pb(OH)$_2$(aq)	17.07
$CaSO_4$(aq)	−2.10	$CaCO_3$(aq)	7.01	Fe^{+3}	−8.49	Pb $(OH)_3^-$	28.07
NaCl(aq)	0.78	KCl(aq)	1.50	CH_4(aq)	144.15	Pb $(CO_3)_2^{2-}$	11.24
$FeCl^+$	0.17	$MgCl^+$	0.14	H_2(aq)	46.11	PbO(aq)	16.98
$FeHCO_3^+$	−2.04	$MgSO_4$(aq)	−2.38	SO_2(aq)	37.57	$PbHCO_3^+$	−2.89
$FeCO_3$(aq)	4.88	$NaSO_4^-$	−0.81	HSO_3^-	39.42	$PbCO_3$(aq)	−3.06
$FeCl_4^{2-}$	1.94	KSO_4^-	−0.88	$PbCl^+$	−1.45	$H_2AsO_4^-$	−21.41
$NaHCO_3$(aq)	−0.17	$NaHSiO_3$(aq)	8.30	$PbCl_2$(aq)	−2.01	$HAsO_4^{2-}$	−14.66

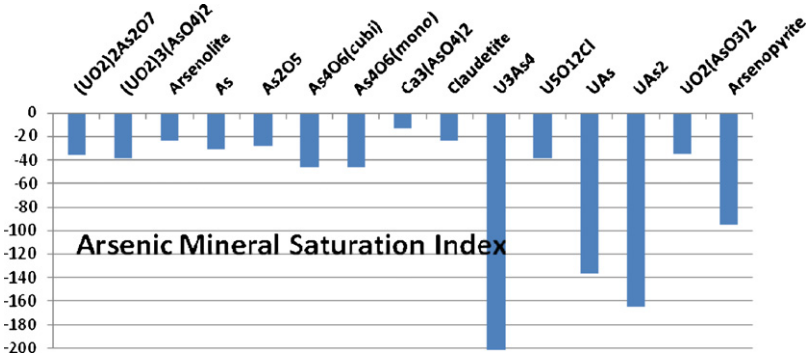

Fig. 8. Saturation indexes of the arsenic related minerals as determined by Phreeqc.

the simulations. Since trends in the μ-XRF mapping discussed in Section 4.4 indicate that As is associated with iron-rich phases, which include clay minerals, a set of sorption reactions for As to the minerals at the site are proposed. For this study, As is assumed to be in the oxidized As(V) form, but concede As(III) may also be present in small amounts and could be a factor to consider in future modeling efforts pending the findings of additional spectroscopic analysis. In the oxidized form, As speciation is dominated by aqueous species $H_2AsO_4^-$ and $HAsO_4^{2-}$. According to the study conducted by Manning and Goldberg (1997) and Goldberg et al. (2008), As aqueous species $H_2AsO_4^-$ and $HAsO_4^{2-}$ tend to sorb onto the iron oxyhydroxides and clay minerals. These minerals may include hematite, (as well as lepidocrocite, goethite, and ferrihydrite), kaolinite, illite, and smectite. Zheng et al. (2009) and Manning and Goldberg (1997) used surface complexation to express the sorption reactions listed below:

Hematite : $\text{Hem\_}H_2AsO_4^- + H_2O \quad \text{Hem\_OH} + H_3AsO_4 \quad \log(K_{int}) = 7.93$ (DixitandHering, 2003)

Hematite : $\text{Hem\_}HAsO_4^{-2} + H_2O + H^+ \quad \text{Hem\_OH} + H_3AsO_4 \quad \log(K_{int}) = 14.52$ (DixitandHering, 2003)

Kaolinite : $\text{Kao\_}HAsO_4^{-2} + H_2O + H^+ \quad \text{Kao\_OH} + H_3AsO_4 \quad \log(K_{int}) = 4.69$ (Goldberg, 2002)

Illite : $\text{Ill\_}H_2AsO_4^- + H_2O \quad \text{Ill\_OH} + H_3AsO_4 \quad \log(K_{int}) = -3.23$ (Goldberg, 2011)

Illite : $\text{Ill\_}HAsO_4^{-2} + H_2O + H^+ \quad \text{Ill\_OH} + H_3AsO_4 \quad \log(K_{int}) = 5.21$ (Goldberg, 2002)

Smectite : $\text{Sme\_}H_2AsO_4^- + H_2O \quad \text{Sme\_OH} + H_3AsO_4 \quad \log(K_{int}) = 4.52$ (Goldberg, 2002)

Aqueous arsenic–carbonate complexes may also affect the sorption process (Kim et al., 2000). Due to the small volume fraction of calcite (0.4% via XRD) this process is currently ignored in the modeling efforts. Cation exchange reactions are also considered as equilibrium reactions in the model in order to evaluate their effect on major cations, pH and trace metals. The Gaines–Thomas convention was adopted for cation exchange (Appelo and Postma, 1993). It should be pointed out that the cation selectivity coefficient is defined with respect to a reference species. By adopting Na^+ as the reference cation, cation exchange reactions are expressed as:

$$Na^+ + 0.5Ca\text{–}X_2 = 0.5Ca^{2+} + Na\text{–}X$$

$$Na^+ + 0.5Mg\text{–}X_2 = 0.5Mg^{2+} + Na\text{–}X$$

$$Na^+ + K\text{–}X = K^+ + Na\text{–}X$$

$$Na^+ + H\text{–}X = H^+ + Na\text{–}X$$

The symbol ( )–X denotes the cation exchanger or an exchange position. Selectivity coefficients of these reactions, $K_{Na/K}$, $K_{Na/Ca}$, $K_{Na/Mg}$, and $K_{Na/H}$, are defined with respect to sodium.

The lower the selectivity, the higher the cation is selected compared to sodium. The cation exchange capacity is defined as CEC (mequiv./100 g of solid). The selectivity coefficients and the CEC are site-specific parameters and not measured for these batch experiments so they are fit parameters in the model.

Table 4
The concentrations (mg/L for all dissolved ions; μg-C/mL for $[CO_2]_{aq}$) and weighting of chemical components at various time-steps from the batch experimental exposure of the Roadcut Lithosome B sample at steady state with the "Background H_2O," reacted with CO_2. Reaction time $t = 0$ h represents the fluid chemistry after the solid and water were allowed to Compositions for the initial reaction fluids representative of the "Background" water and "Saline" water used for the experimental studies are included for comparison.

Species	Background H_2O	Saline H_2O	Reaction time (days)							Weighting
			0.04	1	4	8	11	14	26	
Ca	5.1	222.1	257	277.4	294.5	245.5	234.3	272.9	228.4	0.041
Fe	0.001	0.022	0.007	0.008	0.007	0.009	0.101	2.216	0	1.205
K	0.729	38.57	8.684	8.967	9.212	4.391	4.406	8.28	7.403	0.479
Mg	2.842	220.40	14.16	14.79	15.42	8.911	8.496	14.57	12.06	0.347
Na	73.90	783.90	111.9	110.4	106.6	78.52	77.78	91.41	72.84	0.059
Cl	28	2050	48	45	43	41	40	38	29	0.164
SO4	56.00	333.00	91.53	97	91	81	86	81	63	0.091
U	0.001	0.013	0.003	0.003	0.004	0.004	0.003	0.003	0.003	2.026
As	<DL	0.0002	0.02	0.019	0.017	0.008	0.005	0.004	0.002	0.132
Si	<DL	<DL	6.052	8.442	10.03	3.808	3.761	8.618	6.152	0.411
pH	8.56	6.42	5.99	6.06	6.04	5.97	5.9	5.88	6.03	1.024
CO_2(aq)	–	–	514	532	562	569	545	618	415	0.016

5.2. Comparison of geochemical model to batch laboratory experiments

In order to simulate the As reactive transport at the Chimayo site, geochemical reaction parameters must first be estimated. Fortunately, the batch experiments provided valuable observation data for estimating the related geochemical reaction parameters that are not already well constrained from the literature. By using Toughreact Version 2.0 (Xu et al., 2011) as the forward modeling simulator and PEST (Doherty, 2010) to estimate model parameters, the geochemical reactions described in Section 5.1 were used to simulate our batch experiment scenario of the "Roadcut Lithosome B" sample with background groundwater exposed to CO_2 described in Section 4.1. The experiments measured major ion and trace metal concentrations as a function of time. Included in the simulation were equilibrium complexation reactions, surface/cation exchange sorption reactions, and kinetic mineral dissolution–precipitation.

The observation data of the 26-day batch experiment are listed in Table 4. The numerical methodology for estimating these parameters via inversion involves minimizing the objective function of observation data by $\boldsymbol{J}$,

$$\mathbf{J} = \min \sum_{i=1}^{N} E_i(p)$$
$$E_i(p) = \sum_{l=1}^{L_i} w_{li}^2 (\mathbf{u}_l^i(p) - \tilde{\mathbf{u}}_l^i)^2 \quad (1)$$

where $E_i(p)$ is the sub-objective function from chemical species i, N is the number of chemical species, w_{li} is the weighting coefficient for the lth measurement of the ith species, and $\mathbf{u}_l^i$ and $\tilde{\mathbf{u}}_l^i$ are the simulated and observed concentrations, respectively (see Dai and Samper, 2004; Doherty, 2010). The observation data were weighted by the weighting coefficients shown in Table 4 for each chemical species. The coefficients are computed from using the inverse of the standard deviation of the measurements as explained in Dai and Samper (2004), Hill and Tiedeman (2007) and Dai et al. (2012).

The geochemical parameters for estimation included six selectivity coefficients of cation exchange, cation exchange capacity (CEC), one rate constant for the calcite reactions, and four specific surface areas of the clay minerals described in Section 5.1. These parameters (cation exchange, CEC, calcite reaction, and arsenic sorption) are the parameters expected to be most important for simulating the trends observed during the laboratory experiments and other observations discussed in Section 4. Goldberg (2011) indicates that there is a large amount of uncertainty in the equilibrium constant for the illite/$H_2AsO_4^-$ surface exchange reaction (logK-ill) and the fitting correlation coefficient used to determine this parameter was 0.6. Therefore, this parameter is allowed to vary in the inverse model. A composite sensitivity analysis of the objective function to the 17 geochemical parameters listed in Table 5 was also conducted to explore which parameters are sensitive. Based on the method described in PEST (Doherty, 2010; Dai et al., 2010), the composite sensitivity coefficients were computed for each geochemical parameter. Fig. 9 shows that four parameters are clearly most sensitive: the surface area of calcite (cal-sa), surface area of kaolinite (kao-sa), rate constant of calcite (cal-rfk1) and log equilibrium constant of arsenic sorption onto illite (logK-ill). By examining the model results, it becomes clear why these parameters are critical in matching the experimental results.

The model results of the eight key chemical components are plotted in Fig. 10, and Table 5 shows the estimated parameter values. The four most sensitive parameter estimates are shown in bold in Table 5. When examining Fig. 10, note that the initial concentration of each species in the model is set to the observed initial concentration. Therefore, model and experiment values are guaranteed to match at time zero. The agreement between the evolution of the species concentrations with time for the experiment and the model is of particular interest. The model predicts the change in pH and As concentration as a function of time with some discrepancies. The introduction of CO_2 into the system causes the pH to drop quickly in a short time period but leveling around pH 5.5 due to

Table 5
The estimated geochemical reaction parameters from the batch experiment of Roadcut Lithosome B sample. The most sensitive parameters are shown in bold.

Parameter	Symbol	Estimated value
Cation exchange selectivity coefficient	KNa/H	0.204
	KNa/Ca	0.981
	KNa/Mg	0.002
	KNa/K	0.019
	KNa/Pb	0.615
Cation exchange capacity (mequiv./100 g s)	CEC	1.0
Rate constant (mol/m^2/s)	**cal-rfk1**	**1.73×10^{-6}**
Specific surface area (cm^2/g)	**cal-sa**	**2.05**
	hem-sa	1405.95
	Ill-sa	538.83
	kao-sa	**55.44**
	sme-sa	0.65
	Kfeld-sa	14.68
	qua-sa	26.98
	alb-sa	12.81
	anor-sa	9.53
Equilibrium constant	**logK-ill**	**−10.07**

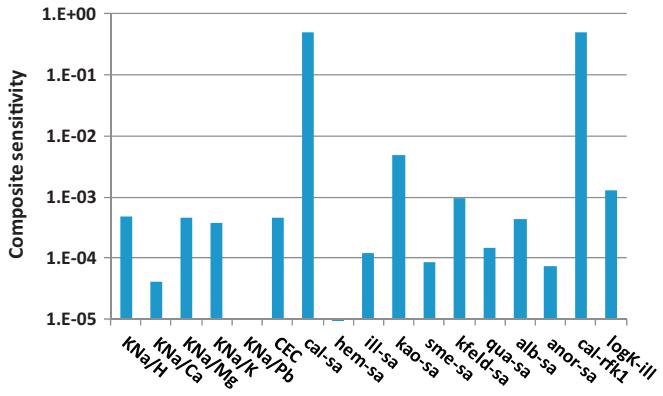

Fig. 9. Sensitivity analysis of the geochemical reactive parameters based on the batch experiment data.

calcite buffering. Since the dissolution of quartz, k-fieldspar, albite and anorthite consumes H^+, it increases the pH values slowly during the later time. This behavior is captured by the model. By interrogating the model, it became clear that cal-rfk1 and the cal-sa are the key parameters in matching the pH behavior. The reaction rate of calcite is fairly well constrained by the literature so we allowed it vary in order to check our parameter estimation methods. The model estimates a cal-rfk1 to be 1.65×10^{-6} mol/m^2/s which is close to the reported value of 1.73×10^{-6} mol/m^2/s (Xu et al., 2011), lending confidence to the parameter estimation exercise.

In the batch experiment As concentrations initially increases quickly and subsequently decreases throughout the remainder of the experiment (see Fig. 4). This release of As may result from the dissolution of trace As-substituted calcite present in the system that dissolves due to the rapid pH drop in the system with addition of CO_2. Other possibilities include As desorption from oxides and/or clays. For time points where the pH decreases from ~8 to ~6, aqueous As also is observed to decrease slightly from 0.020 mg/L to 0.017 mg/L (within 0.04 days), however pH slowly increases after the initial drop throughout the remainder of the experiment while As concentrations continue to decrease. Wilken and Digiulio (2010) notes that anionic metalloids such as As may be more effectively sorbed at lower pH; which is generally consistent with

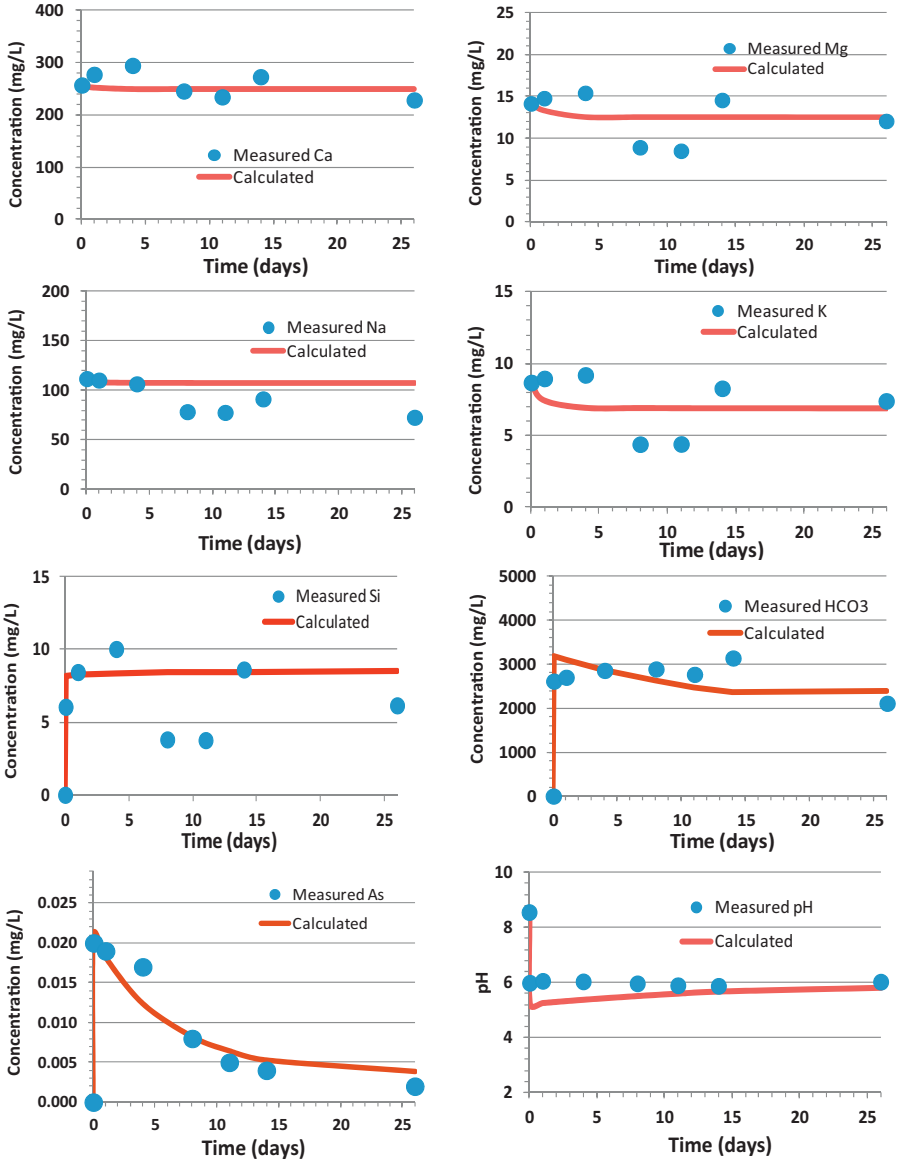

Fig. 10. Inverse modeling results of the batch experiment of Roadcut Lithosome B sample.

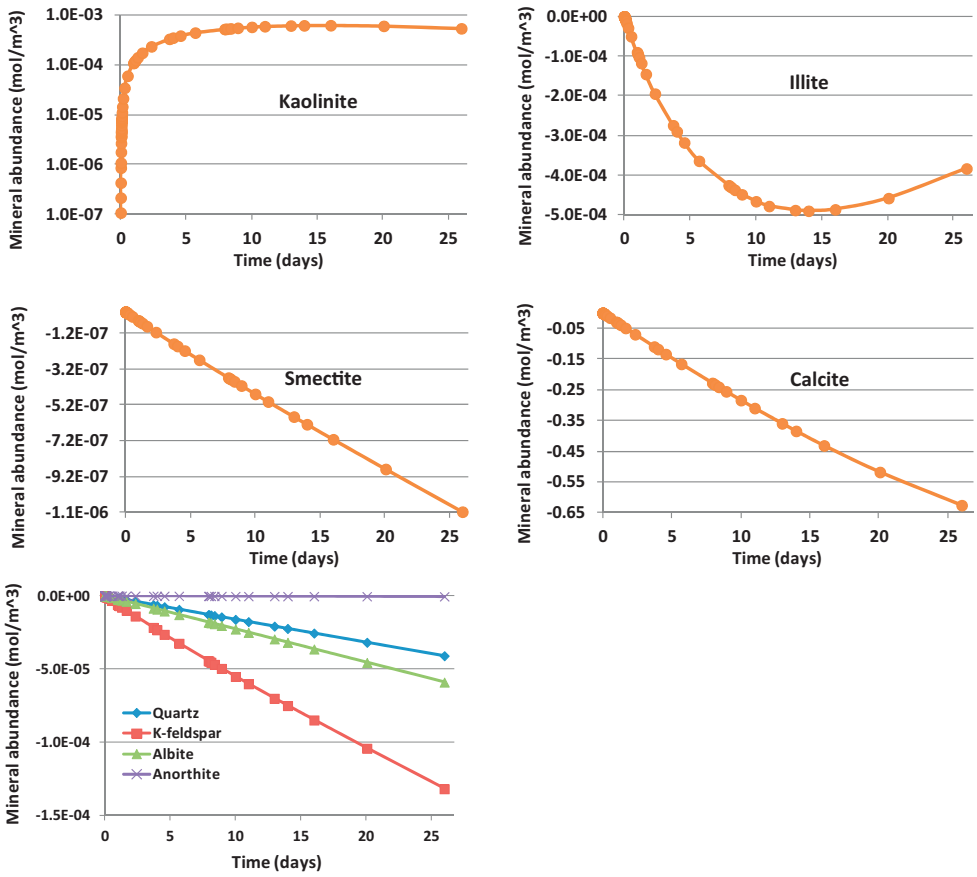

Fig. 11. Simulated precipitation (positive concentration) and dissolution (negative) of minerals during the batch experiment (hematite is not shown because of negligible abundance change).

our experimental and modeling trends. Additionally, as the pH decreases and H^+ concentration increases due to the introduction of CO_2, our model shows that precipitation of clay minerals (e.g. kaolinite) is favored due the mineral precipitation/dissolution reaction shown in Section 5.1 (Fig. 11). Determining experimentally whether kaonilite actually precipitated is difficult since only a small amount of kaolinite is expected to form. Attempts to measure major ion chemistry changes due to precipitation (e.g. Si) or collection of precipitate was inconclusive or not practical. However, it would appear that even a small amount of precipitation combined with sorption could be a significant contributor controlling As concentrations in the model. Alternative conceptual models are also possible to describe the behavior of these experiments. For example, sorption kinetics could also be responsible for As decreasing with time. The sensitivity of As concentration to small amounts of precipitation and major ion chemistry demonstrates the grand challenge of determining the fate of trace metals in the environment. Although illite and smectite were dissolved during the batch experiment, both of them still provided plentiful sorption sites due to their large volume fractions.

Given the potential for additional sorption sites to become available during the course of Chimayo sediment reactions with CO_2, in addition to sorption sites already available through the sediment's mineral assemblage, we focused on As sorption to clay surfaces as a controlling factor on As geochemistry throughout the experiment. Our model includes four key parameters for controlling As adsorption; specifically, surface areas for illite (ill-sa), kaonilite (kao-sa) and smectite (sme-sa) and the equilibrium constant for As sorption onto illite. These parameters influence the model predictions due to the relatively large volume fractions of illite and smectite, 43.4% and 20.2%, respectively (see Table 1b). Although kaonilite has a small volume fraction (1.5%), it precipitates to add more sorption sites and the sorbed As onto kaonilite sites increases with time in the numerical model (see Fig. 12). Fig. 12 also shows that sorption is strongly a function of pH. Therefore, at close to time zero, pH quickly changes resulting in fast sorption/desorption of As in this early time-frame.

The behavior of the As is similar to observations by Smyth et al. (2006) for aquifer samples exposed to CO_2 for two weeks. Specifically, As concentration is initially high due to the introduction of CO_2 followed by a gradual decrease in As concentration. Smyth et al. (2006) found two types of responses to CO_2, which they defined as: (1) "Type 1" ions (B, Ba, Ca, Co, K, Mg, Mn, Sr and Zn), elements whose concentrations increased rapidly in solution and then either remained constant or increased slowly over time, and (2) "Type II' ions (Al, As, Cs, Cu, Fe, Mo, Ni, Rb, U and V), elements whose concentrations increased rapidly followed by a gradual decrease. One hypothesis suggested by Smyth et al. (2006) for 'Type II' is that the formation of new mineral surfaces may scavenge trace elements from solution. This process is consistent with what is captured by the model in this study to fit the decrease of As concentration at the later time of the experiment. In the model, As decreases gradually due to sorption on existing and fresh sorption sites resulting from precipitation of additional clay minerals during the experiment (see Fig. 11). Other studies have shown that trace metal scavenging is important at natural analog sites (e.g. Aiuppa et al., 2005).

6. Reactive transport model

A simplified field-scale reactive transport model was constructed using the reactions developed in Section 4.1 to simulate a hypothetical 1D flow path through the Chimayo system. Fig. 13

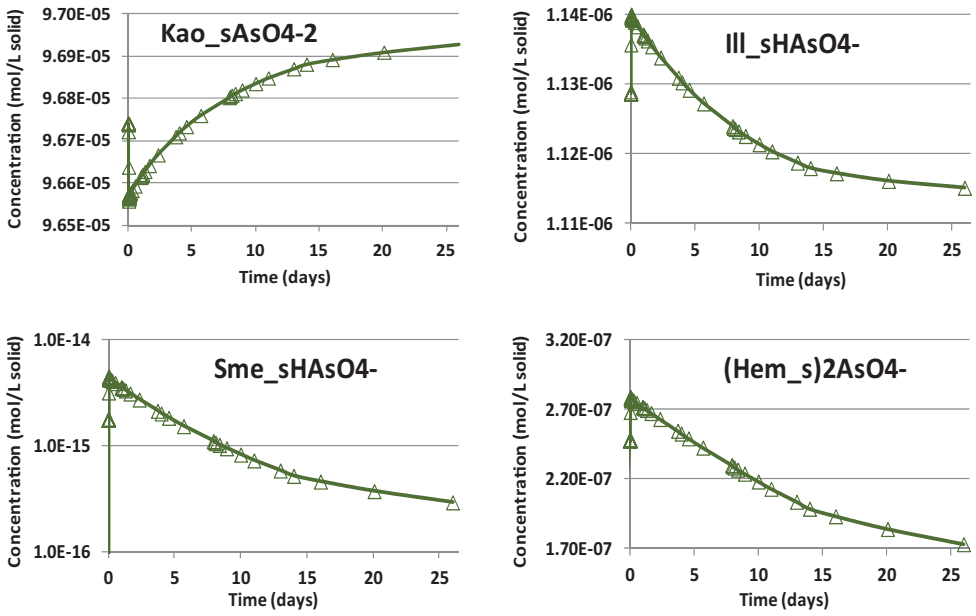

Fig. 12. Simulated adsorbed As onto sorption mineral sites during the batch experiment Please note that the *y*-axes values are different for each mineral phase in order to illustrate trends.

shows the conceptual model where CO_2 leaks from the subsurface through a deep carbonate aquifer into the shallow sandstone aquifer. The one-dimensional reactive transport model has a height of 120 m. The CO_2 leaks from the deep aquifer where the concentrations of chemical components are unknown. Vertical head gradient data does not exist at the site so an estimated flow rate was assumed to demonstrate the effect of the reactions on the transport of species. The head is known at several deep and shallow wells at the site. The difference in head is about 5 m on average between the deep and shallow wells. A flow rate in the column was calculated by using the head difference between the shallow and deep aquifers for a mean conductivity of 0.1 m/day for the model length of 120 m. This results in a flow rate of 4.82×10^{-5} kg/s entering the column. In the field-scale model an average volume fraction of 28% is assigned for illite by considering the heterogeneity of the mineral distributions in the Chimayo site (see Table 1a). The other minerals are also assigned their average weight fractions (Table 1b).

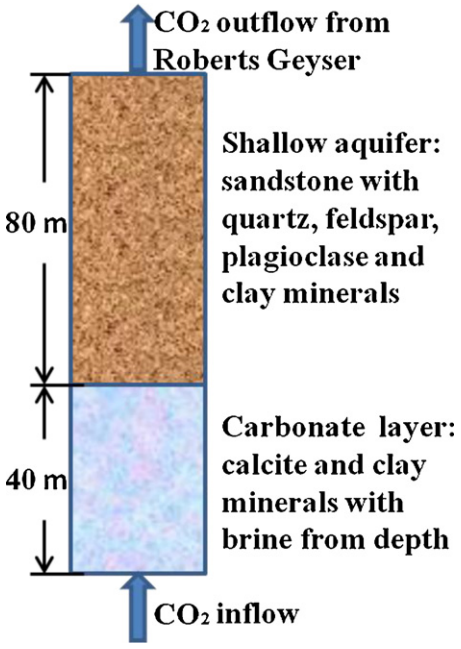

Fig. 13. Conceptual model for field-scale reactive transport simulations.

By using geochemical parameters from the batch experiments described in Section 4.2, the recharge concentrations (entering the column) of the major chemical components such as As, Ca, Mg, Na, K and Cl were estimated to attempt to match the Well 17 (e.g., Fig. 1) chemical signature that is assumed to be the "true" concentrations at top of the 1D column (Fig. 13). Since the time scale (thousands years) is much larger than that of the batch experiment, calcite dissolution/precipitation is assumed to be equilibrium. Other minerals have rate constants much less (more than six orders of magnitude less) than that of calcite, and their dissolution/precipitation reactions are still kinetically controlled. The goal is to determine how species concentrations evolve along the flow path due to the chemical reactions identified in Section 5. The objective function is also defined by equation 1. For this parameter estimation exercise the simulated concentrations are defined as the steady state simulated concentration at Well 17 (the top of the model in Fig. 13). However, rather than varying reaction parameters as in the previous section, recharge concentrations are the estimated parameters. The geochemical processes simulated in this field-scale reactive transport model are assumed to be the same as those used in simulating the batch experiments. In fact, most of the reactive transport parameters are scale dependent (Dai et al., 2009). Understanding and accounting for the scaling effects of the geochemical parameters is a topic of ongoing work.

As expected, similar processes occur in the two sets of simulations since the same set of reactions occur. When CO_2 inflows into the model from the deep aquifer, the pH in the shallow aquifer drops quickly with time but levels out around 6 due to buffering by calcite. The aqueous As concentration in the shallow aquifer initially increases due to the transport (advection, dispersion and diffusion) of As from the deep aquifer. When As concentration increases, adsorption onto clay minerals increases due to surface complexation with clays and hematite. As the pH decreases and H^+ concentration increases, precipitation of clay minerals is favored providing more sorption sites, which enhances As sorption onto the clay minerals and reduces solution concentration. Finally the

Table 6
Comparison of the observed concentration, computed concentration and the estimated recharge (inflow) concentration (mg/L).

Species (mg/L)	Shallow aquifer		Deep aquifer
	Observed	Computed	Estimated
pH	6.4	6.0	6.419
Ca	529.1	520.6	1669.5
Mg	207.1	207.5	207.7
Na	1143.0	1145.3	1163.0
K	40.3	40.4	40.4
Cl	648.8	648.4	648.5
HCO_3	2977.0	2949.1	4702.8
As	0.0188	0.0189	0.0398

transport of As from the deep fluid source reaches equilibrium with As sorption onto the clay minerals in the simulated Chimayo aquifer. The clay minerals illite and smectite dominate in the As sorption process due to their relatively large volume fraction.

For the species that are either conservative (e.g. Cl) or only participate in equilibrium sorption reactions (e.g. As), the estimated recharge concentration are similar to the observed data of Well 17 since these reactions do not change the total aqueous concentration once steady state conditions are reached. This was an expected result and confirms that the parameter estimation routine was working correctly. Table 6 confirms that the estimated recharge concentrations for Cl and As are very similar to the calculated and observed concentrations at the top of the column. However, equilibrium sorption reactions can delay the travel time of these species which is important for assessing shallow groundwater impacts for these species. Fig. 14 shows that As exiting the top of the column is indeed strongly retarded compared to the conservative tracer Cl. The transport of trace metals to the shallow aquifer is critical for assessing shallow subsurface impacts due to brine or CO_2 intrusion. The effective retardation of trace metals is an important parameter to evaluate in performance assessment studies (Viswanathan et al., 2008) and is dependent on multiple coupled reactions.

As expected, estimated deep aquifer Ca, H^+ and HCO_3^- concentrations are different from the observed shallow concentrations (Table 6). For species participating in mineral precipitation/dissolution reactions (e.g. Na, Ca, H^+, HCO_3, and Mg), the estimated recharge concentration may be different from the observed concentration since mineral reactions can change the total aqueous concentrations of these species as they transport along the flow path. Ion exchange reactions also result in some sorption of the major ions, as seen in Fig. 15, although the retardation for these major ions is far less than for As. The reactive transport simulations presented in this manuscript are greatly simplified with the assumption of a 1D flow path and by using geochemical parameters from the batch modeling studies that are likely scale

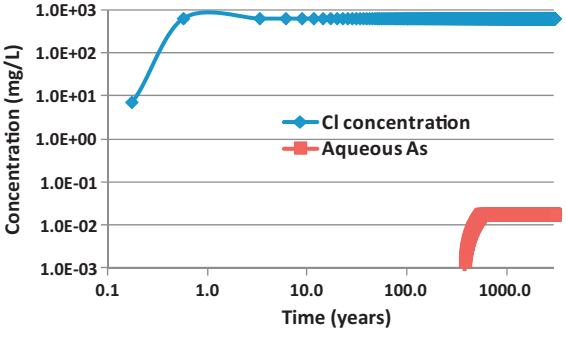

Fig. 14. Simulated travel times for conservative solute Cl and sorbing As exiting the column.

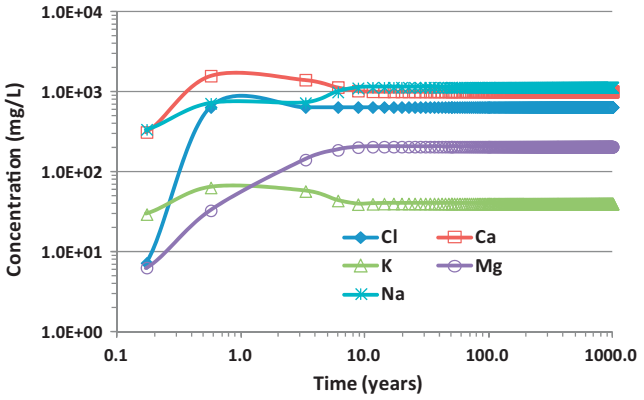

Fig. 15. Simulated travel times for conservative solute Cl and other major ions exiting the column.

dependent. However, the simulations are intended to show how different reaction types affect the transport of various species in the Chimayo groundwater. The simulations show that predicting trace metal migration is dependent on multiple coupled processes, and due to low concentrations of these trace metals, many processes can greatly affect their fate in the natural environment.

7. Conclusions

This manuscript presents a suite of experimental and modeling techniques combined with field observations to gather multiple lines of evidence for processes controlling the fate of As in Chimayo sediments and groundwater. The focus of this work was to combine a diverse suite of techniques ranging from micro-scale geochemical characterization to basin-scale reactive transport modeling in order the address the challenging problem of CO_2 storage on trace metal fate. On an individual level some results are preliminary and warrant additional investigation. However, coupled with the body of results, all pieces of data are important for informing the higher-level processes being considered for site-scale reactive transport scenarios. The study shows that small changes to major aqueous ions or solid phases can have a large impact on trace metal concentrations making prediction of trace metal fate a very challenging problem requiring multiple lines of evidence to understand their behavior.

More thorough investigations for certain analyses (e.g., synchrotron studies) are ongoing. Batch experiments and materials characterization, including XRD, SEM, and μ-XRF, shows that As is most likely initially associated with Fe-rich phases such as clays or oxides in the shallow Chimayo sediments. Batch laboratory experiments with Chimayo sediments and groundwater showed that pH initially decreases as CO_2 is introduced into the experimental system, and the system is almost immediately buffered by calcite. The introduction of CO_2 causes an immediate increase in As at the beginning of the experiment relative to CO_2-free controls. Arsenic concentrations decrease in solution as a function of time relative to the initial value. A batch geochemical model was developed to simulate these experiments. The model correctly predicts the pH drop once CO_2 is introduced into the experiment. In the model, the surface area of kaolinite proved to be the key parameter in simulating the drop in As concentration as a function of time. Kaolinite precipitates during the simulation allowing for additional sorption sites as a function of time resulting in the slow decrease in As concentration. The amount of kaolinite precipitation is small and cannot be confirmed in the experiments due to detection limits. This is a common problem with predicting the fate of trace metals where small changes in major ions or solid-phases can have a large impact on trace metal concentration. Therefore, identifying the controlling

mechanisms with regards to trace metals is very challenging. The mechanism simulated by the model can be viewed as trace element "scavenging" due to sorption associated with secondary mineral precipitation of illite. In the literature, "scavenging" has been shown to be an important process with regard to trace metals. At the field scale, As transport is retarded due to sorption reactions which will impact the likelihood of As reaching the accessible environment in a performance assessment for CO_2 sequestration study.

Sorption processes were a major focus of this study based on the studies by Goldberg et al. (2008) and this has had a major impacts on how the data were modeled in this analysis. In future work, we plan to study the additional possibility of sorption–reduction as another process controlling As and trace metal mobility at the Chimayo site. This process may be significant in that, As sorption (and to a lesser extent Pb, and U) with Fe-rich phases (including but not limited to clays) appears to play a major role in As fate in the shallow subsurface at Chimayo. Localized structural site-to-site electron exchange has been shown to be potentially significant related to sorption–reduction of U (Ilton et al., 2004; Singer et al., 2009; Chakraborty et al., 2010), and may be significant for several other redox-sensitive elements (Peterson et al., 1997; Felmy et al., 2011). While this process has been shown by Chakraborty et al. (2011) to not be as significant for As on phases such as biotite, it could have additional impacts on how to predict controls on metal mobility in the Chimayo system in general.

In summary, the data show that arsenic upwells from the deep aquifer with CO_2 and then (under the oxidizing conditions of the aquifer) adsorbs to iron-bearing minerals (e.g. clays) at the Chimayo site, retarding As transport in the shallow groundwater. Other trace elements such as U or Pb may or may not be controlled by completely different processes. Therefore, the risk assessment of each trace element of concern will require a fairly complex analysis to determine the key parameters that affect its fate at the site. A combination of laboratory and field observations will have to be joined with geochemical modeling to identify the key parameters of interest. As opposed to major ions, trace elements exist at such low concentrations that processes such as scavenging by secondary minerals can greatly affect their fate and transport in the subsurface. The simulations presented represent a small range of conditions and the transport model was greatly simplified. At a CO_2 sequestration site, factors such as leakage pathways and aquifer heterogeneity need to be considered to make a proper assessment of risk in shallow aquifers due to the transport of trace elements in brines and reactions with CO_2.

Acknowledgements

This work was supported by US DOE through the Zero Emission Research & Technology II project and the NETL Strategic Center for Coal. We would like to thank the three reviewers for greatly improving the manuscript. We thank Debbie Burse for performing aqua regia digestions, Kristen Carlisle for coordinating experimental fluids analyses, and Jennifer LeBel for performing laboratory experimental work with CO_2. We also thank Hongwu Xu of LANL for the detailed quantitative XRD analyses. The U.S. Environmental Protection Agency through its Office of Research and Development participated in the data collection and analysis of a portion of the research described here. It has not been subject to agency review and therefore does not necessarily reflect the views of the agency. No official endorsement should be inferred. Portions of this work were performed at GeoSoilEnviroCARS (Sector 13), Advanced Photon Source (APS), Argonne National Laboratory. GeoSoilEnviroCARS is supported by the National Science Foundation – Earth Sciences (EAR-0622171) and Department of Energy – Geosciences (DE-FG02-94ER14466). Use of the advanced photon source was supported by the U.S. Department of Energy, Office of Science, Office of Basic Energy Sciences, under contract no. DE-AC02-06CH11357.

References

Aiuppa, A., Federico, C., Allard, P., Gurrieri, S., Valenza, M., 2005. Trace metal modeling of groundwater-gas-rock interactions in a volcanic aquifer: Mount Vesuvius, Southern Italy. Chemical Geology 216, 289–311.

Appelo, C.A.J., Postma, D., 1993. Geochemistry, Groundwater and Pollution. A.A. Balkema, Brookfield, VT.

Apps, J.A., Zheng, L., Yang, Y., Xu, T., Birkolzer, J.T., 2010. Evaluation of potential changes in groundwater quality in response to CO_2 leakage from deep geologic storage. Transport in Porous Media 82, 215–246.

Bachu, S., 2000. Sequestration of CO_2 in geological media: criteria and approach for site selection in response to climate change. Energy Conversion and Management 41, 953–970.

Chakraborty, S., Favre, F., Banerjee, D., Scheinost, A., Mullet, M., Ehrhardt, J., Brendle, J., Vidal, L., Charlet, L., 2010. U(VI) sorption and reduction by Fe(II) sorbed on Montmorillonite. Environmental Science and Technology 44, 3779–3785.

Chakraborty, S., Bardelli, F., Mullet, M., Greneche, J., Varma, S., Ehrdardt, J., Banerjee, D., Charlet, L., 2011. Spectroscopic studies of arsenic retention onto biotite. Chemical Geology 281, 83–92.

Chipera, S.J., Bish, D.L., 2002. FULLPAT: a full pattern quantitative analysis program for X-ray powder diffraction using measured and calculated patterns. Journal of Applied Crystallography 35, 744–749.

Cumming, K.A., 1997. Hydrogeochemistry of Groundwater in Chimayo, NM, M.S. Northern Arizona University, Flagstaff, AZ, pp. 117.

Dai, Z., Samper, J., 2004. Inverse problem of multicomponent reactive chemical transport in porous media: formulation and applications. Water Resource Research 40, W07407, http://dx.doi.org/10.1029/2004WR003248.

Dai, Z., Wolfsberg, A.V., Lu, Z., Deng, H., 2009. Scale dependence of sorption coefficients for radionuclide transport in saturated fractured rock. Geophysical Research Letters 36, L01403, http://dx.doi.org/10.1029/2008GL036516.

Dai, Z., Keating, E., Gable, C.W., Levitt, D., Heikoop, J., Simmons, A., 2010. Stepwise inversion of a groundwater flow model with multi-scale observation data. Hydrogeology Journal 18, 607–624, http://dx.doi.org/10.1007/s10040-009-0543-y.

Dai, Z., Wolfsberg, A., Reimus, P., Deng, H., Kwicklis, E., Ding, M., Ware, D., Ye, M., 2012. Identification of sorption processes and parameters for radionuclide transport in fractured rock. Journal of Hydrology 414–415, 220–230.

Dixit, S., Hering, J.G., 2003. Effects of arsenate reduction and iron oxide transformation on arsenic mobility. Environmental Science and Technology 37, 4182–4189.

Doherty, J., 2010. PEST, Model-Independent Parameter Estimation. Watermark Computing, Corinda, Australia, 122 p.

EPA, 2009. List of Contaminants & their Maximum Contaminant Level (MCLs). Website: http://water.epa.gov/drink/contaminants/index.cfm#List, EPA 816-F-09-0004, May.

Felmy, A.R., Ilton, E.S., Rosso, K.M., et al., 2011. Interfacial reactivity of radionuclides: emerging paradigms from molecular-level observations. Mineralogical Magazine 75 (4), 2379–2391.

Goldberg, S., 2002. Competitive adsorption of arsenate and arsenite on oxides and clay minerals. Soil Science Society of America Journal 66, 413–421.

Goldberg, S., 2011. The optimizations for the intrinsic equilibrium constants of As(V) illite adsorption, personal communication.

Goldberg, S., Hyun, S., Lee, L.S., 2008. Chemical modeling of arsenic(III, V) and selenium(IV, VI) adsorption by soils surrounding ash disposal facilities. Vadose Zone Journal 7 (4), 1231–1238.

Hakala, J.A., Fimmen, R.L., Chin, Y.-P., Agrawal, S., Ward, C.P., 2009. Assessment of the geochemical reactivity of Fe-DOM complexes in wetland sediment pore waters using a nitroaromatic probe compound. Geochimica et Cosmochimica Acta 73, 1382–1393.

Hereford, A.G., Keating, E.H., Guthrie, G.D., Zhu, C., 2007. Reactions and reaction rates in the regional aquifer beneath the Pajarito Plateau, north-central New Mexico, USA. Environmental Geology 52, 965–977.

Hill, M.C., Tiedeman, C.R., 2007. Effective Calibration of Ground Water Models, with Analysis of Data, Sensitivities, Predictions, and Uncertainty. John Wiely, New York, p. 455.

Ilton, E.S., Haiduc, A., Moses, C.O., Heald, S.M., Elbert, D.C., Veblen, D.R., 2004. Heterogeneous reduction of uranyl by micas: crystal chemical and solution controls. Geochimica et Cosmochimica Acta 68 (11), 2417–2435.

IPCC Climate Change 2007: The physical sciences basis; contribution of Working Group I to the fourth assessment report of the Intergovernmental Panel on Climate Change; approved a the 10th Session of Working Group I of the IPCC, Paris, 2007.

Keating, E.H., Warren, R., 1999. Geochemistry of the Regional Aquifer. Los Alamos National Laboratory Report, pp. 35.

Keating, E.H., Fessenden, J., Kanjorski, N., Koning, D.J., Pawar, R.J., 2010. The impact of CO_2 on shallow groundwater chemistry: observations at a natural analog site and implications for carbon sequestration. Environmental Earth Sciences.

Kharaka, Y.K., Cole, D.R., Hovorka, S., Gunter, W.D., Knauss, K.G., Freifeld, B.M., 2006. Gas–water–rock interactions in Frio Formation following CO_2 injection: implications for the storage of greenhouse gases in sedimentary basins. Geology 34, 577–580.

Kim, M.J., Nriagu, J., Haack, S., 2000. Carbonate ions and arsenic dissolution in groundwater. Environmental Science and Technology 34, 3094–3100.
Manning, B.A., Goldberg, S., 1997. Adsorption and stability of arsenic(III) at the clay mineral–water interface. Environmental Science and Technology 31, 2005–2011.
Parkhurst, D.L., Appelo, C.A.J., 1999. User's guide to PHREEQC (version 2)—a computer program for speciation, batch-reaction, one-dimensional transport, and inverse geochemical calculations: U.S. Geological Survey Water-Resources Investigations Report 99-4259, 312 pp.
Peterson, M.L., Brown, G.E., Parks, G.A., Stein, C.L., 1997. Differential redox and sorption of Cr(III/IV) on natural silicate and oxide minerals: EXAFS and XANES results. Geochimica et Cosmochimica Acta 61 (16), 3399–3412.
Singer, D.M., Maher, K., Brown, G.E., 2009. Uranyl-chlorite sorption/desorption: evaluation of different U(VI) sequestration processes. Geochimica et Cosmochimica Acta 73, 5989–6007.
Smyth, R.C., Holtz, M.H., Guillot, S.N., 2006. Assessing impacts to groundwater from CO_2-flooding of SACROC and Claytonville oil fields in West Texas. Presented at the 2006 UIC Conference of the Groundwater Protection Council, Austin, Texas, 24 January.
Stauffer, P.H., Keating, G.N., Middleton, R.S., Viswanathan, H.S., Berchtold, K.A., Singh, R.P., Pawar, R.J., Mancino, A., 2011. Greening coal: breakthroughs and challenges in carbon capture and storage. Environmental Science and Technology 45, 8597–8604.
Viswanathan, H.S., Pawar, R.J., Stauffer, P.H., Kaszuba, J.P., Carey, J.W., Olsen, S.C., Keating, G.N., Kavetski, D., Guthrie, G.D., 2008. Development of a hybrid process and system model for the assessment of wellbore leakage at a geologic CO_2 sequestration site. Environmental Science and Technology 42, 7280–7286.
Wilken, R.T., Digiulio, D.C., 2010. Geochemical impacts to groundwater from geologic carbon sequestration: controls on pH and inorganic carbon concentrations from reaction path and kinetic modeling. Environmental Science and Technology 44, 4821–4827.
Xu, T., Apps, J.A., Pruess, K., 2003. Reactive geochemical transport simulation to study mineral trapping for CO_2 disposal in deep arenaceous formations. Journal of Geophysical Research 108 (B2), 2071, http://dx.doi.org/10.1029/2002JB001979.
Xu, T., Apps, J.A., Pruess, K., 2005. Mineral sequestration of carbon dioxide in a sandstone-shale system. Chemical Geology 217 (3–4), 295–318, http://dx.doi.org/10.1016/j.chemgeo.2004.12.015.
Xu, T., Sonnenthal, E.L., Spycher, N., Pruess, K., 2006. TOUGHREACT – a simulation program for non-isothermal multiphase reactive geochemical transport in variably saturated geologic media: applications to geothermal injectivity and CO_2 geological sequestration. Computers & Geosciences 32 (2), 145–165.
Xu, T., Spycher, N., Sonnenthal, E., Zhang, G., Zheng, L., Pruess, K., 2011. TOUGHREACT Version 2.0: a simulator for subsurface reactive transport under non-isothermal multiphase flow conditions. Computers & Geosciences 37 (6), 763–774.
Zheng, L., Apps, J.A., Zhang, Y., Xu, T., Birkholzer, J.T., 2009. On mobilization of lead and arsenic in groundwater in response to CO_2 leakage from deep geological storage. Chemical Geology.